

# Optimal Inferential Control of Convolutional Neural Networks

Ali Vaziri and Huazhen Fang

**Abstract**—Convolutional neural networks (CNNs) have achieved remarkable success in representing and simulating complex spatio-temporal dynamic systems within the burgeoning field of scientific machine learning. However, optimal control of CNNs poses a formidable challenge, because the ultra-high dimensionality and strong nonlinearity inherent in CNNs render them resistant to traditional gradient-based optimal control techniques. To tackle the challenge, we propose an optimal inferential control framework for CNNs that represent a complex spatio-temporal system, which sequentially infers the best control decisions based on the specified control objectives. This reformulation opens up the utilization of sequential Monte Carlo sampling, which is efficient in searching through high-dimensional spaces for nonlinear inference. We specifically leverage ensemble Kalman smoothing, a sequential Monte Carlo algorithm, to take advantage of its computational efficiency for nonlinear high-dimensional systems. Further, to harness graphics processing units (GPUs) to accelerate the computation, we develop a new sequential ensemble Kalman smoother based on matrix variate distributions. The smoother is capable of directly handling matrix-based inputs and outputs of CNNs without vectorization to fit with the parallelized computing architecture of GPUs. Numerical experiments show that the proposed approach is effective in controlling spatio-temporal systems with high-dimensional state and control spaces. All the code and data are available at <https://github.com/Alivaziri/Optimal-Inferential-Control-of-CNNs>.

## I. INTRODUCTION

Spatio-temporal dynamic systems arise in various scientific and engineering disciplines, including flow dynamics, heat transfer, nuclear fusion, and natural hazards. Control of such systems has attracted decades-spanning interest, with a substantial body of research. Model-based control has been a prevailing approach. Its success springs from incorporating mathematical models into feedback control design to effectively handle complex dynamics. Most models have been constructed using partial differential equations (PDEs) [1]. These PDE-based models are expressive and structurally efficient, but often demand great amounts of time and labor to derive and validate for real-world systems. Recently, machine learning has emerged as a powerful approach for modeling spatio-temporal systems, thanks to its capacity of extracting accurate representations of a system’s behavior from abundant data, while allowing for fast training and validation [2], [3]. In this regard, convolutional neural networks (CNNs) have proven especially useful [2], [3]. CNNs are a class of multi-layer deep learning models distinguished by the inclusion of convolutional layers. These layers apply convolution operations to capture spatial correlations and dependencies

A. Vaziri and H. Fang are with the Department of Mechanical Engineering, University of Kansas, Lawrence, KS 66045, USA. Email: {alivaziri, fang}@ku.edu

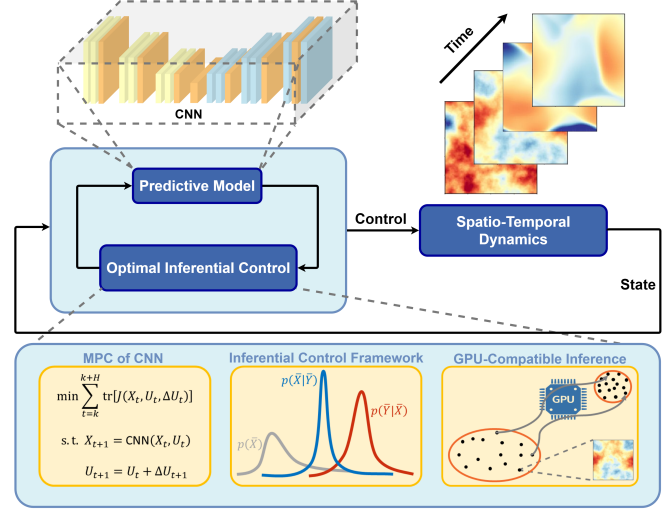


Fig. 1: The OIC framework for control of CNNs.

within data. With this characteristic, CNNs are suitable for describing complex spatio-temporal dynamics. They have been used to solve PDEs through the physics-informed machine learning paradigm [2], [4], and have also achieved remarkable success in building data-driven surrogates across numerous domains, e.g., weather forecasting, traffic modeling, and aerodynamics [5]–[7].

A CNN-based spatio-temporal dynamic model typically takes a matrix-based state-space form:

$$X_{k+1} = \text{CNN}_{\theta}(X_k, U_k), \quad (1)$$

where  $X_k \in \mathbb{R}^{n \times m}$  is the spatio-temporal field at time  $k$ ,  $U_k \in \mathbb{R}^{l \times m}$  is the control input, and  $\theta$  is the trainable parameters of the CNN. For (1), optimal control is an interesting new problem, central to applications that will adopt CNN-based modeling. However, this problem is non-trivial, because the ultra-high dimensions, strong nonlinearity, and nonconvexity of  $\text{CNN}_{\theta}$  will lead to extremely complex optimization landscapes, for which gradient-based optimization solvers will perform poorly or fail easily. No study has been available to investigate the challenge, to our knowledge.

To fill in this gap, we develop an *optimal inferential control* (OIC) framework as shown in Fig. 1 to enable optimal control of CNNs, through the following two contributions.

- We propose to address optimal control of CNNs via probabilistic inference. This perspective centers around inferring or estimating the best control actions from the control objectives and constraints, setting up the basis for the OIC framework, opening up the use of nonlinear state estimation of (1).

- To computationally implement OIC for (1), we propose harnessing the power of Monte Carlo sampling for inference and further combining it with the computational prowess of graphics processing units (GPUs). To this end, we develop a sequential ensemble Kalman smoother (EnKS). This EnKS uniquely builds on matrix variate distributions and can exploit GPUs' multi-dimensional array operations to accelerate computation considerably.

The OIC framework marks the first attempt for control of CNNs while departing from gradient-based optimal control methods. It also shows the significant, yet still rarely tapped, potential of sampling-based inference and GPU to achieve computationally efficient control of highly complex systems.

## II. RELATED WORK

This section provides a literature review of the topics related with the proposed study.

**Control of PDE systems.** PDE control is a challenging problem that has driven many influential studies. For boundary control, the backstepping method has found important use in dealing with many types of PDEs, linear or nonlinear, and with time delays, disturbances, or parametric uncertainty [8]–[10]. Other important methods include the Riesz basis approach and Lyapunov design [11], [12]. Optimal control of PDEs dates back to the 1970s [13]. The works in [14]–[17] investigate linear quadratic and sum-of-squares control for PDEs, and model predictive control (MPC) has also gained traction [18], [19]. To mitigate computation, one can leverage Koopman operator theory to build data-driven linear predictors for nonlinear PDEs [20]–[22], or use model order reduction to obtain low-order models [23], [24].

**MPC of neural network dynamic models.** The likely first study on this topic is [25], which applies dynamic matrix control, a precursor of MPC, to a neural-network-modeled pH process. Since then, growing research has led to diverse methods and applications spanning from chemical processes to robotics [26]–[31]. However, gradient-based optimization, the de facto solver, struggles to offer sufficient computation and optimization performance for deep multi-layer neural networks. To alleviate the issue, relatively efficient solvers are custom-designed in [31], and input-convex neural networks are used in [32]. Alternatively, sampling has shown intriguing promise. A simple sampling technique in [33] is to randomly generate many candidate control decision sequences and then pick the sequence that leads to minimum costs. In our prior study [34], [35], we propose to use particle filtering/smoothing to solve MPC of neural networks after translating it into a probabilistic inference problem; our further study [36] shows that improved sampling schemes for particle filtering/smoothing can speed up computation greatly. Despite these advances, CNN's ultra-high dimensionality and complicated structure present unprecedented challenges for MPC, leaving this problem widely open.

**Connections between inference and control.** The idea of control via inference echoes some existing theories and methods. The first related concept is the control/estimation duality, which was first established in the 1960s between

Kalman smoothing and linear quadratic regulation [37]. Duality for nonlinear systems is often elusive, but the formulation of optimal control and inference problems dual to each other in this case has attracted recurring interest [38]–[40]. In the field of robotics, variational inference and message passing have found their way into computing optimal control problems efficiently [41], [42]. Monte Carlo sampling, along with its variants, excels in performing probabilistic inference in high-dimensional spaces and with complex nonlinearity. In this regard, particle filtering has shown to be useful for MPC of nonlinear systems [34]–[36], [43]. Reinforcement learning can also be treated as probabilistic inference [44], which allows to use a wide array of estimation tools to perform learning.

## III. PROBLEM SETUP

Given (1), we formulate an MPC problem in this section. First, consider the following cost function for the purpose of reference tracking:

$$J(X_{k:k+H}, U_{k:k+H}, \Delta U_{k:k+H}) = \sum_{t=k}^{k+H} \text{tr} [J(X_t, U_t, \Delta U_t)],$$

where  $H$  is the control horizon length, and

$$J(X_t, U_t, \Delta U_t) = (X_t - X^{\text{ref}})^\top R^{-1} (X_t - X^{\text{ref}}) + (U_t - U^{\text{ref}})^\top Q_U^{-1} (U_t - U^{\text{ref}}) + \Delta U_{t+1}^\top Q_{\Delta U}^{-1} \Delta U_{t+1}.$$

Here,  $X^{\text{ref}}$  and  $U^{\text{ref}}$  are the references for  $X_t$  and  $U_t$ , respectively, at which the model in (1) is at steady state satisfying  $X^{\text{ref}} = \text{CNN}_\theta(X^{\text{ref}}, U^{\text{ref}})$ ;  $\Delta U_t$  is the incremental control input defined as

$$\Delta U_{t+1} = U_{t+1} - U_t. \quad (2)$$

Further,  $R$ ,  $Q_U$ , and  $Q_{\Delta U} > 0$  are weighting matrices. We now set up an MPC problem to control the model in (1):

$$\begin{aligned} \min \quad & J(X_{k:k+H}, U_{k:k+H}, \Delta U_{k:k+H}), \\ \text{s.t.} \quad & X_{t+1} = \text{CNN}_\theta(X_t, U_t), \\ & U_{t+1} = U_t + \Delta U_{t+1}, \quad t = k, \dots, k+H. \end{aligned} \quad (3)$$

This problem seeks the optimal control actions within each receding horizon to steer  $X_t$  towards  $X^{\text{ref}}$  while minimizing the control effort. Its matrix-based format, which differs from conventional vector-based MPC formulations, results from controlling spatio-temporal dynamics represented by  $\text{CNN}_\theta$ . Yet, if performing vectorization, we can find that

$$\begin{aligned} \text{tr} [J(X_t, U_t, \Delta U_t)] = & \\ & \text{vec} (X_t - X^{\text{ref}})^\top (I \otimes R)^{-1} \text{vec} (X_t - X^{\text{ref}}) \\ & + \text{vec} (U_t - U^{\text{ref}})^\top (I \otimes Q_U)^{-1} \text{vec} (U_t - U^{\text{ref}}) \\ & + \text{vec} (\Delta U_t)^\top (I \otimes Q_{\Delta U})^{-1} \text{vec} (\Delta U_t), \end{aligned}$$

which is identical to the quadratic cost in vector-based reference-tracking MPC. Here,  $\otimes$  is the Kronecker product.

MPC has been generally addressed by gradient-based optimization. However, attempts to apply this approach to (3) are feasible only for small-scale CNNs. For spatio-temporal

systems, a CNN-based model often  $X_t$  and/or  $U_t$  with tens of thousands of dimensions. Furthermore, CNNs present significant nonconvexity and nonlinearity. With these factors, the MPC problem in (3) is unyielding to gradient-based optimization. As an effective solution is still absent from the literature, we propose a new framework, referred to as *optimal inferential control*, to tackle this challenge. Our pursuit involves transforming the problem in (3) into a sequential inference problem and then developing a highly efficient, GPU-compatible EnKS approach to conduct the inference.

#### IV. THE OPTIMAL INFERENCE CONTROL FRAMEWORK

This section derives the optimal inferential control framework for MPC of CNNs. To execute the framework, we develop an EnKS approach aligned with GPU computing for computational benefits.

##### A. Problem Transformation

The MPC problem in (3) embraces a reformulation as a probabilistic inference problem. To show this, we consider a virtual auxiliary system taking the form of

$$\begin{cases} X_{t+1} = \text{CNN}_\theta(X_t, U_t), \\ U_{t+1} = U_t + \Delta U_{t+1}, \\ \Delta U_{t+1} = W_t, \\ X^{\text{ref}} = X_t + V_{X,t}, \\ U^{\text{ref}} = U_t + V_{U,t}, \end{cases} \quad (4)$$

for  $t = k, \dots, k+H$ . In above,  $X_t$ ,  $U_t$ , and  $\Delta U_t$  together form the virtual state,  $X^{\text{ref}}$  and  $U^{\text{ref}}$  represent the virtual observation; further,  $W_t$ ,  $V_{X,t}$  and  $V_{U,t}$  are additive noises following matrix normal distributions [45] (see Appendix):

$$W_t \sim \mathcal{MN}(0; \Sigma_W, \Psi_W), \quad V_{X,t} \sim \mathcal{MN}(0; \Sigma_{V_X}, \Psi_{V_X}), \\ V_{U,t} \sim \mathcal{MN}(0; \Sigma_{V_U}, \Psi_{V_U}).$$

Intuitively, the virtual system in (4) replicates the dynamics of the original system, but is observed to behave optimally over the upcoming horizon  $[k, k+H]$ . Based on this insight, if we estimate  $X_t$ ,  $U_t$ , and  $\Delta U_t$  for  $t = k, \dots, k+H$  using the virtual observation of the optimal behavior as the evidence, then the best control actions will be identified. To proceed forward, we rewrite (4) compactly as

$$\begin{cases} \bar{X}_{t+1} = f_{\text{CNN}}(\bar{X}_t) + \bar{W}_t, \\ \bar{Y}_t = H\bar{X}_t + \bar{V}_t, \end{cases} \quad (5)$$

where

$$\bar{X}_t = \begin{bmatrix} X_t \\ U_t \\ \Delta U_t \end{bmatrix}, \quad \bar{Y}_t = \begin{bmatrix} X^{\text{ref}} \\ U^{\text{ref}} \end{bmatrix}, \quad \bar{W}_t = \begin{bmatrix} 0 \\ W_t \\ W_t \end{bmatrix}, \\ \bar{V}_t = \begin{bmatrix} V_{X,t} \\ V_{U,t} \end{bmatrix}, \quad H = \begin{bmatrix} I & 0 & 0 \\ 0 & I & 0 \end{bmatrix},$$

and  $f_{\text{CNN}}(\cdot)$  is evident from the context. To identify the state  $\bar{X}_t$  for (5), we take the method of maximum a posteriori estimation, which yields

$$\hat{\bar{X}}_{k:k+H} = \arg \max_{\bar{X}_{k:k+H}} \log p(\bar{X}_{k:k+H} | \bar{Y}_{k:k+H}), \quad (6)$$

where  $p(\bar{X}_{k:k+H} | \bar{Y}_{k:k+H})$  is the posterior distribution of  $\bar{X}_{k:k+H}$  given  $\bar{Y}_{k:k+H}$ , and  $\hat{\bar{X}}_{k:k+H}$  is the estimate. This is a state smoothing problem in the literature on probabilistic inference. The following theorem shows an equivalence between (6) and the original MPC problem in (3).

*Theorem 1:* Suppose that  $W_t$ ,  $V_{X,t}$  and  $V_{U,t}$  are mutually independent, and that  $\Sigma_{V_X} \otimes \Psi_{V_X} = I \otimes R$ ,  $\Sigma_{V_U} \otimes \Psi_{V_U} = I \otimes Q_U$ , and  $\Sigma_W \otimes \Psi_W = I \otimes Q_{\Delta U}$ . Then, the problems in (3) and (6) share the same optima.

*Proof:* By Bayes' rule and the Markovianity of (5), we have

$$p(\bar{X}_{k:k+H} | \bar{Y}_{k:k+H}) \propto \prod_{t=k}^{k+H} p(\bar{Y}_t | \bar{X}_t) \prod_{t=k+1}^{k+H} p(\bar{X}_t | \bar{X}_{t-1}) \\ \times p(\bar{X}_k).$$

The log-likelihood then is given by

$$\log p(\bar{X}_{k:k+H} | \bar{Y}_{k:k+H}) \propto \sum_{t=k}^{k+H} \log p(X^{\text{ref}} | X_t) \\ + \sum_{t=k}^{k+H} \log p(U^{\text{ref}} | U_t) + \sum_{t=k+1}^{k+H} \log p(\Delta U_t),$$

as  $p(\bar{Y}_t | \bar{X}_t) = p(X^{\text{ref}} | X_t) p(U^{\text{ref}} | U_t)$ ,  $p(\bar{X}_t | \bar{X}_{t-1}) = p(\Delta U_t)$ , and  $\bar{X}_k$  is known at time  $k$ . Given (4),  $X^{\text{ref}} | X_t \sim \mathcal{MN}(X_t; \Sigma_{V_X}, \Psi_{V_X})$ ,  $U^{\text{ref}} | U_t \sim \mathcal{MN}(U_t; \Sigma_{V_U}, \Psi_{V_U})$ ,  $\Delta U_t \sim \mathcal{MN}(0; \Sigma_W, \Psi_W)$ . This implies

$$\log p(\bar{X}_{k:k+H} | \bar{Y}_{k:k+H}) \propto - \sum_{t=k}^{k+H} \text{tr} \left[ \Sigma_t^{-1} \Delta U_t \Psi_W^{-1} \Delta U_t^\top \right. \\ \left. + \Sigma_{V_X}^{-1} (X_t - X^{\text{ref}}) \Psi_{V_X}^{-1} (X_t - X^{\text{ref}})^\top \right. \\ \left. + \Sigma_{V_U}^{-1} (U_t - U^{\text{ref}}) \Psi_{V_U}^{-1} (U_t - U^{\text{ref}})^\top \right] \\ = - \sum_{t=k}^{k+H} \left[ \text{vec}(X_t - X^{\text{ref}})^\top (\Sigma_{V_X} \otimes \Psi_{V_X})^{-1} \text{vec}(X_t - X^{\text{ref}}) \right. \\ \left. + \text{vec}(U_t - U^{\text{ref}})^\top (\Sigma_{V_U} \otimes \Psi_{V_U})^{-1} \text{vec}(U_t - U^{\text{ref}}) \right. \\ \left. + \text{vec}(\Delta U_t)^\top (\Sigma_W \otimes \Psi_W)^{-1} \text{vec}(\Delta U_t) \right],$$

which is the opposite of  $J(X_{k:k+H}, U_{k:k+H}, \Delta U_{k:k+H})$  in the problem (3) when  $\Sigma_{V_X} \otimes \Psi_{V_X} = I \otimes R$ ,  $\Sigma_{V_U} \otimes \Psi_{V_U} = I \otimes Q_U$ , and  $\Sigma_W \otimes \Psi_W = I \otimes Q_{\Delta U}$ . This completes the proof.  $\blacksquare$

Theorem 1 illustrates the viability of treating nonlinear MPC as probabilistic state estimation. This perspective not only resonates with the well-known control/estimation duality, but also sets a basis for performing MPC via nonlinear estimation. Next, we will translate the perspective into the development of a state estimation method to deal with MPC for CNNs. Before moving forward, a special case of Theorem 1 is noteworthy—the equivalence between (3) and (6) holds when  $\Psi_{V_X} = R$ ,  $\Psi_{V_U} = Q_U$ , and  $\Psi_W = Q_{\Delta U}$ , and  $\Sigma_{V_X}$ ,  $\Sigma_{V_U}$ , and  $\Sigma_W = I$ . This knowledge can help one readily set up a state estimation problem that is consistent with the MPC problem in (3).

## B. MPC via GPU-Compatible EnKS

While various nonlinear state smoothing methods exist, they will face tremendous computational difficulties if applied directly to the problem in (6), due to the ultra-high dimensions of the CNN model. We will address this issue in a twofold way. First, we choose EnKS to address the smoothing problem in (6). EnKS is arguably the most computationally efficient smoothing method for high-dimensional nonlinear systems [46], [47]. This merit stems from its design that integrates sampling-based Monte Carlo simulation with Kalman-type update in estimation. Specifically, a single-pass EnKS technique proposed in [47] is considered here, which computes smoothed estimates sequentially in just a single forward pass. This compares to other methods requiring two passes, forward filtering and backward smoothing, and causing more tedious computation. Second, we intend to exploit GPUs to achieve rapid computation for smoothing. GPUs are designed to support parallel computation and especially efficient in handling matrix operations. We thus will transform the single-pass EnKS to make it compatible with the matrix-format model in (5) and fit GPUs.

The idea of single-pass smoothing to deal with the problem in (6) pursues a sequential update from  $p(\bar{X}_{k:t-1} | \bar{Y}_{k:t-1})$  to  $p(\bar{X}_{k:t} | \bar{Y}_{k:t})$  for  $t = k, \dots, k + H$ , governed by

$$p(\bar{X}_{k:t} | \bar{Y}_{k:t}) = p(\bar{Y}_t | \bar{X}_t) p(\bar{X}_t | \bar{X}_{t-1}) p(\bar{X}_{k:t-1} | \bar{Y}_{k:t-1}). \quad (7)$$

However, there is no closed-form solution to (7) for a nonlinear system. To make the problem tractable, we define  $\mathcal{X}_t = \bar{X}_{k:t}$  and  $\mathcal{Y}_t = \bar{Y}_{k:t}$  for notational simplicity, and approximate  $p(\mathcal{X}_t, \bar{Y}_t | \mathcal{Y}_{t-1})$  as a matrix normal distribution:

$$\begin{bmatrix} \mathcal{X}_{t|t-1} \\ \bar{Y}_{t|t-1} \end{bmatrix} \sim \mathcal{MN} \left( \begin{bmatrix} \hat{\mathcal{X}}_{t|t-1} \\ \hat{\bar{Y}}_{t|t-1} \end{bmatrix}, \begin{bmatrix} \Sigma_{t|t-1}^{\mathcal{X}} & \Sigma_{t|t-1}^{\mathcal{X}\bar{Y}} \\ \left(\Sigma_{t|t-1}^{\mathcal{X}\bar{Y}}\right)^\top & \Sigma_{t|t-1}^{\bar{Y}} \end{bmatrix} \otimes \Psi \right), \quad (8)$$

where  $\hat{\mathcal{X}}$  and  $\hat{\bar{Y}}$  are the means of  $\mathcal{X}$  and  $\bar{Y}$ , and  $\Sigma$  are covariance matrices. Given (7)-(8), the marginal conditional probability distribution  $p(\mathcal{X}_t | \mathcal{Y}_t)$  is also matrix-normal:

$$\mathcal{X}_t | \mathcal{Y}_t \sim \mathcal{MN} \left( \hat{\mathcal{X}}_{t|t}, \Sigma_{t|t}^{\mathcal{X}} \otimes \Psi \right), \quad (9)$$

where

$$\hat{\mathcal{X}}_{t|t} = \hat{\mathcal{X}}_{t|t-1} + \Sigma_{t|t-1}^{\mathcal{X}\bar{Y}} \left( \Sigma_{t|t-1}^{\bar{Y}} \right)^{-1} \left( \bar{Y}_t - \hat{\bar{Y}}_{t|t-1} \right), \quad (10a)$$

$$\Sigma_{t|t}^{\mathcal{X}} = \Sigma_{t|t-1}^{\mathcal{X}} + \Sigma_{t|t-1}^{\mathcal{X}\bar{Y}} \left( \Sigma_{t|t-1}^{\bar{Y}} \right)^{-1} \left( \Sigma_{t|t-1}^{\mathcal{X}\bar{Y}} \right)^\top. \quad (10b)$$

This shows a closed-form Kalman-type smoothing update of  $p(\mathcal{X}_t | \mathcal{Y}_t)$  in the matrix-normal setting. By applying it recursively through time, we will get a single-pass smoother.

Next, to implement (10), we take a Monte Carlo approach, using an ensemble of samples to approximate the probability distributions of interest and then performing the update over the samples. In this line, we let  $p(\mathcal{X}_t | \mathcal{Y}_{t-1})$  be approximately represented by the samples  $\{\mathcal{X}_{t|t-1}^i, i = 1, \dots, N\}$ . The

sample mean for  $p(\mathcal{X}_t | \mathcal{Y}_{t-1})$  is then given by

$$\hat{\mathcal{X}}_{t|t-1} = \frac{1}{N} \sum_{i=1}^N \mathcal{X}_{t|t-1}^i, \quad (11)$$

Further, we use  $\mathcal{X}_{t|t-1}^i$  to compute the samples that weakly approximate  $p(\bar{Y}_t | \mathcal{Y}_{t-1})$ :

$$\bar{Y}_{t|t-1}^i = H \bar{X}_{t|t-1}^i + \bar{V}_t^i, \quad (12)$$

for  $i = 1, \dots, N$ , where  $\bar{V}_t^i$  is drawn from the distributions of  $V_{X,t}$  and  $V_{U,t}$ . Then, we compute

$$\hat{\bar{Y}}_{t|t-1} = \sum_{i=1}^N \bar{Y}_{t|t-1}^i, \quad (13a)$$

$$\Sigma_{t|t-1}^{\bar{Y}} = \frac{\lambda}{N} \sum_{i=1}^N \left( \bar{Y}_{t|t-1}^i - \hat{\bar{Y}}_{t|t-1} \right) \left( \bar{Y}_{t|t-1}^i - \hat{\bar{Y}}_{t|t-1} \right)^\top, \quad (13b)$$

$$\Sigma_{t|t-1}^{\mathcal{X}\bar{Y}} = \frac{\lambda}{N} \sum_{i=1}^N \left( \mathcal{X}_{t|t-1}^i - \hat{\mathcal{X}}_{t|t-1} \right) \left( \bar{Y}_{t|t-1}^i - \hat{\bar{Y}}_{t|t-1} \right)^\top, \quad (13c)$$

where  $\lambda = 1/\text{tr}(\Psi)$ . By (10a), the Kalman smoothing update is executed for  $\mathcal{X}_{t|t-1}^i$  for  $i = 1, \dots, N$  to find out

$$\hat{\mathcal{X}}_{t|t} = \frac{1}{N} \sum_{i=1}^N \mathcal{X}_{t|t}^i, \quad (14a)$$

$$\mathcal{X}_{t|t}^i = \mathcal{X}_{t|t-1}^i + \Sigma_{t|t-1}^{\mathcal{X}\bar{Y}} \left( \Sigma_{t|t-1}^{\bar{Y}} \right)^{-1} \left( \bar{Y}_t - \bar{Y}_{t|t-1}^i \right), \quad (14b)$$

$$\Sigma_{t|t}^{\mathcal{X}} = \frac{\lambda}{N} \sum_{i=1}^N \left( \mathcal{X}_{t|t}^i - \hat{\mathcal{X}}_{t|t} \right) \left( \mathcal{X}_{t|t}^i - \hat{\mathcal{X}}_{t|t} \right)^\top, \quad (14c)$$

where  $\{\mathcal{X}_{t|t}^i, i = 1, \dots, N\}$  weakly approximate  $p(\mathcal{X}_t | \mathcal{Y}_t)$ . Note that  $\lambda$  in  $\Sigma_{t|t-1}^{\bar{Y}}$  and  $\Sigma_{t|t-1}^{\mathcal{X}\bar{Y}}$  will cancel each other in (14b). Going forward, we use these samples to make prediction to create an ensemble for  $p(\mathcal{X}_{t+1} | \mathcal{Y}_t)$ :

$$\hat{\bar{X}}_{t+1|t} = \sum_{i=1}^N \bar{X}_{t+1|t}^i, \quad (15a)$$

$$\bar{X}_{t+1|t}^i = f_{\text{CNN}} \left( \bar{X}_{t|t}^i \right) + \bar{W}_t^i, \quad (15b)$$

$$\mathcal{X}_{t+1|t}^i \leftarrow \left( \mathcal{X}_{t|t}^i, \bar{X}_{t+1|t}^i \right), \quad \hat{\mathcal{X}}_{t+1|t} \leftarrow \left( \hat{\mathcal{X}}_{t|t}, \hat{\bar{X}}_{t+1|t} \right), \quad (15c)$$

$$\Sigma_{t+1|t}^{\bar{X}} = \frac{\lambda}{N} \sum_{i=1}^N \left( \bar{X}_{t+1|t}^i - \hat{\bar{X}}_{t+1|t} \right) \left( \bar{X}_{t+1|t}^i - \hat{\bar{X}}_{t+1|t} \right)^\top, \quad (15d)$$

$$\Sigma_{t+1|t}^{\mathcal{X}\bar{X}} = \frac{\lambda}{N} \sum_{i=1}^N \left( \mathcal{X}_{t+1|t}^i - \hat{\mathcal{X}}_{t+1|t} \right) \left( \bar{X}_{t+1|t}^i - \hat{\bar{X}}_{t+1|t} \right)^\top, \quad (15e)$$

$$\Sigma_{t+1|t}^{\mathcal{X}} = \begin{bmatrix} \Sigma_{t|t}^{\mathcal{X}} & \Sigma_{t+1|t}^{\mathcal{X}\bar{X}} \\ \left(\Sigma_{t+1|t}^{\mathcal{X}\bar{X}}\right)^\top & \Sigma_{t+1|t}^{\bar{X}} \end{bmatrix}, \quad (15f)$$

---

**Algorithm 1** Kalman-MPC: MPC of CNNs via GPU-Compatible Single-Pass EnKS
 

---

- 1: Set up the MPC problem in (3) for the CNN-based spatio-temporal model in (1)
- 2: Set up the virtual system in (5)
- 3: **for**  $k = 1, 2, \dots, \mathbf{do}$
- 4:   Initialize  $\bar{X}_{k|k}^i$  for  $i = 1, \dots, N$
- 5:   **for**  $t = k + 1, \dots, k + H$  **do**
  - // Prediction
  - 6:    Compute  $\bar{X}_{t|t-1}^i$  and  $\hat{X}_{t|t-1}$  via (15a)-(15b)
  - 7:    Obtain  $\mathcal{X}_{t|t-1}^i$  and  $\hat{\mathcal{X}}_{t|t-1}$  by concatenation via (15c)
  - 8:    Compute  $\Sigma_{t|t-1}^{\mathcal{X}}$ ,  $\Sigma_{t|t-1}^{\mathcal{X}\bar{X}}$ , and  $\Sigma_{t|t-1}^{\mathcal{X}}$  via (15d)-(15f)
  - // Update
  - 9:    Compute  $\bar{Y}_{t|t-1}^i$ ,  $\hat{Y}_{t|t-1}$ ,  $\Sigma_{t|t-1}^{\bar{Y}}$ , and  $\Sigma_{t|t-1}^{\mathcal{X}\bar{Y}}$  via (12)-(13)
  - 10:    Compute  $\mathcal{X}_{t|t}^i$  and  $\hat{\mathcal{X}}_{t|t}$  via (14a)-(14b)
  - 11:    Compute  $\Sigma_{t|t}^{\mathcal{X}}$  via (14c)
  - 12:    **end for**
  - 13:    Extract  $\hat{X}_{k|k:k+H}$  from  $\hat{\mathcal{X}}_{k+H|k+H}$ , and  $\hat{U}_{k|k:k+H}$  from  $\hat{\mathcal{X}}_{k|k:k+H}$
  - 14:    Apply  $\hat{U}_{k|k:k+H}$  to the spatio-temporal system
  - 15:    **end for**

Note: Lines 8 and 11 are skippable.

---

where the sample  $\bar{W}_t^i$  is taken from the distribution of  $\bar{W}_t$ , and  $\leftarrow$  stands for the concatenating operation. Note that (15) joins with (11) to close the loop for recursion.

The above presents a prediction-update EnKS procedure to perform MPC. The prediction is performed via (15), and the update via (12)-(14). These two steps run alternately and sequentially over time to complete the smoothing in a single forward pass. We name the algorithm as `Kalman-MPC`, summarizing it in Algorithm 1. In practice, one can choose not to execute (14c) and (15d)-(15f) to save computation and storage, if they are not interested to determine  $\Sigma_{t|t}^{\mathcal{X}}$ ,  $\Sigma_{t+1|t}^{\bar{X}}$  and  $\Sigma_{t+1|t}^{\mathcal{X}\bar{X}}$ , which play no role in the update.

### C. Discussion

The above optimal inferential control framework is the first solution for optimal control of CNN-modeled spatio-temporal dynamic systems. Embodying the framework is the `Kalman-MPC` algorithm, which attains computational tractability for several reasons. First, it leverages Monte Carlo sampling to search through the ultra-high-dimensional state and control spaces, and EnKS provides a principled way to ensure the efficiency in sampling. Second, the single-pass EnKS technique partitions a large-scale search problem into smaller sequential searches, effectively limiting the search space at every step and restraining the computation. Finally, the `Kalman-MPC` algorithm, by matrix-based design, well utilizes GPU's multi-dimensional array operations and parallelized computing capabilities.

The framework can be expanded to include state/input constraints. Suppose supplementing the original MPC in (3) with a constraint  $g(\bar{X}_t, \bar{U}_t) \leq 0$ , where  $g(\cdot, \cdot)$  is a scalar-output function without loss of generality. We introduce a virtual observation  $z_t$  to measure the constraint satisfaction:

$z_t = \phi(g(\bar{X}_t, \bar{U}_t)) + \varepsilon_t$ , where  $\phi(x)$  is a barrier function taking 0 if  $x \leq 0$  and  $\infty$  otherwise, and  $\varepsilon_t$  is a small additive noise. By design,  $z_t$  is close to 0 if the constraint is met, and  $\infty$  otherwise. We can add  $z_t$  to be part of  $\bar{Y}_t$  in (5), while setting its reference to be 0 to ensure the awareness of the constraint in the estimation. In practical implementation, one can use a softplus function to make an adjustable barrier:  $\phi(x) = \frac{1}{\alpha} \ln(1 + e^{\beta x})$ , where  $\alpha, \beta > 0$ .

The setup of  $\bar{X}_t$  requires  $X_t$ ,  $U_t$ , and  $\Delta U_t$  in (5) to have the same number of columns. This is due to the need of using matrix normal distributions and the marginalization property in (9)-(10) to obtain the Kalman smoothing update in the single-pass EnKS. However, a system's actual control input, denoted as  $u_t$ , may have fewer columns. To meet the requirement, we can augment  $u_t$  to  $U_t$  by  $U_t = u_t T$ , where  $T$  is a right-transformation matrix with  $TT^\top > 0$ . If  $u_t$  is a column vector, a simple choice for  $T$  is  $T = [1 \ \dots \ 1]$ , which implies repeating  $u_t$  in the column dimension. When the Kalman-MPC algorithm returns  $\hat{U}_{k|k:k+H}$  at time  $k$ , we can reconstruct  $\hat{u}_{k|k:k+H}$  by  $\hat{u}_{k|k:k+H} = \hat{U}_{k|k:k+H} T^\top (TT^\top)^{-1}$ .

Note that  $R$ ,  $Q_U$ , and  $Q_{\Delta U}$  may need some tuning in the implementation stage, as they impact the sampling-based search within the state and control spaces. Overall, the tuning should introduce an appropriate level of randomness to balance exploration and exploitation in the sampling. This can be done by adjusting  $R$ ,  $Q_U$ , and  $Q_{\Delta U}$  proportionately without changing the ratios between them.

## V. NUMERICAL EXPERIMENTS

This section evaluates the `Kalman-MPC` algorithm by simulation. A CNN-based model is learned first from the 2-D Burgers' PDE, following the approach in [48]. We then use the `Kalman-MPC` algorithm to compute the optimal control actions based on the CNN model, and then apply the control input to the PDE. All the simulations were conducted on Google Colab using an NVIDIA A100-SXM4-40GB GPU and PyTorch's CUDA library.

The 2-D Burgers' PDE is given by

$$\frac{\partial \varphi}{\partial t} + \varphi \cdot \nabla \varphi = \nu \nabla^2 \varphi + f, \quad (16)$$

where  $\varphi(x, y, t) = (\varphi_x, \varphi_y)$  is the velocity field over the domain of  $\Omega = [0, 1] \times [0, 1]$ ,  $f$  is the external force,  $\nu = 0.005$  is the viscosity coefficient. To train the CNN model, (16) is discretized with a  $200 \times 200$  grid and solved with a time step of  $dt = 0.001$ . We consider two control setups: 1) boundary control, in which  $f$  on the boundary  $y = 1$ , including  $f_1$  and  $f_2$ , are the control input variables, and 2) pointwise control, in which  $f$  at every spatial point is a control input variable. The purpose of the second setup is to test the scalability of the `Kalman-MPC` algorithm to very high control dimensions. The `Kalman-MPC` algorithm runs on a horizon of  $H = 5$  and uses  $N = 100$  samples in the receding-horizon smoothing process.

Beginning with the boundary control setup, we desire to steer  $\varphi$  towards the reference  $\psi^{\text{ref}} = 1$ , and define the root

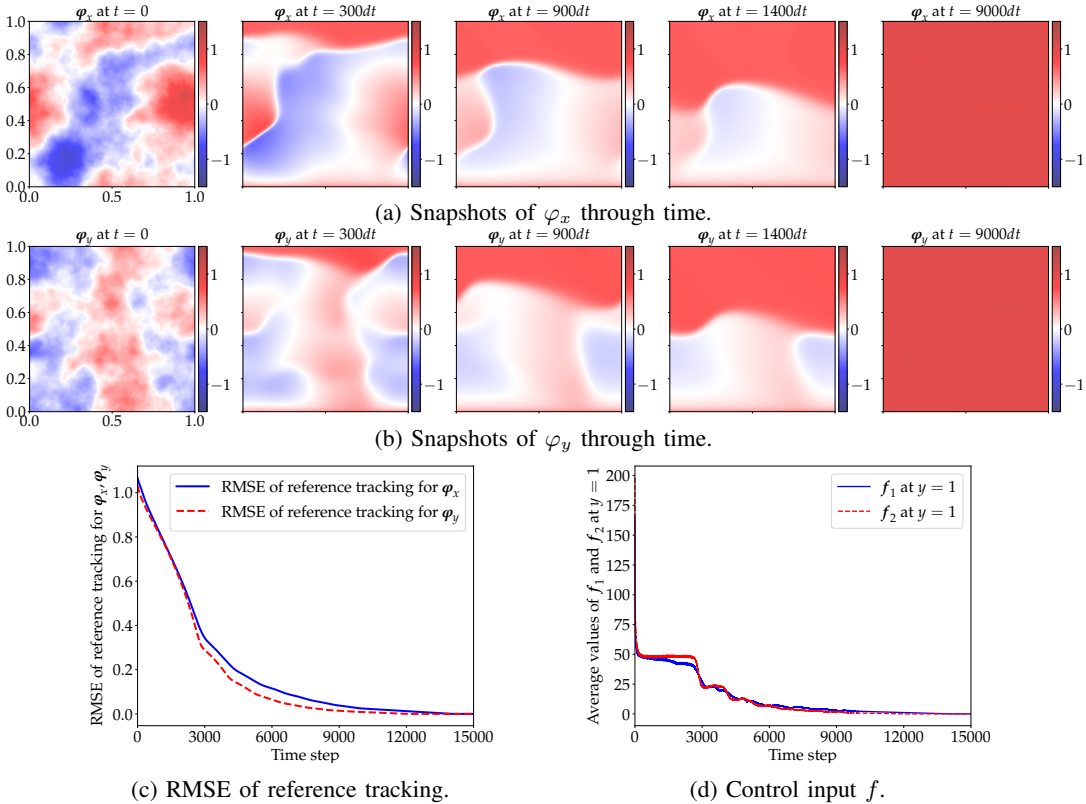


Fig. 2: Control of the 2-D Burgers' PDE on  $200 \times 200$  grid by Kalman-MPC.

TABLE I: Comparison between the vector-based and GPU-compatible versions of Kalman-MPC.

Grid size		$2 \times 64 \times 64$	$2 \times 80 \times 80$	$2 \times 128 \times 128$	$2 \times 200 \times 200$
Vector-based Kalman-MPC	Time	2.55 s	9.51 s	—	—
	Storage	26.7 GB	36.1 GB	Memory outage	Memory outage
GPU-compatible Kalman-MPC	Time	0.42 s	0.51 s	0.954 s	2.097 s
	Storage	2.2 GB	3.2 GB	4.9 GB	12.0 GB

mean squared error (RMSE) in reference tracking as

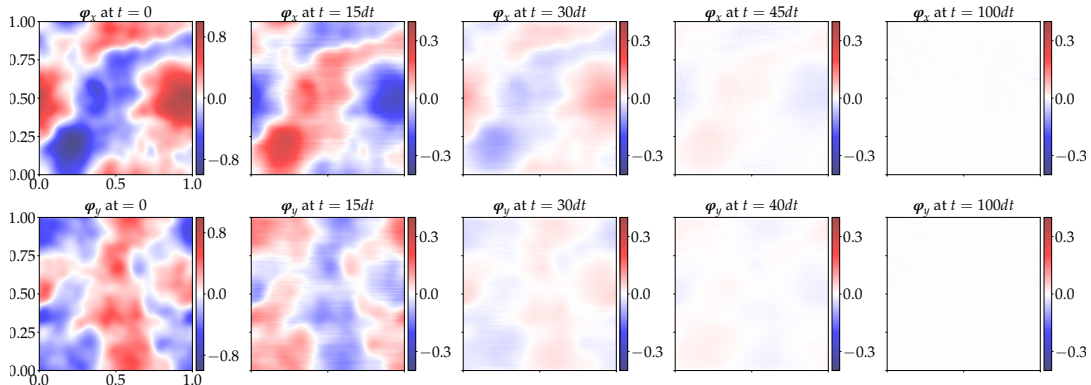
$$\text{RMSE} = \frac{\|\varphi - \varphi^{\text{ref}}\|_F^2}{\text{Total number of grid points}},$$

where  $\|\cdot\|_F$  is the Frobenius norm of a matrix. Figs. 2a-2b show the snapshots of the velocity field at different time steps under control by the Kalman-MPC algorithm. Initially,  $\varphi_x$  and  $\varphi_y$  vary arbitrarily over the domain, but both converge to  $\psi^{\text{ref}}$ . This trend is also displayed in Fig. 2c, in which the RMSE declines to zero. The control input variables  $f_1$  and  $f_2$  also converge toward zero, as shown in Fig. 2d, because  $(\varphi = 1, f = 0)$  is a stable equilibrium point for (16).

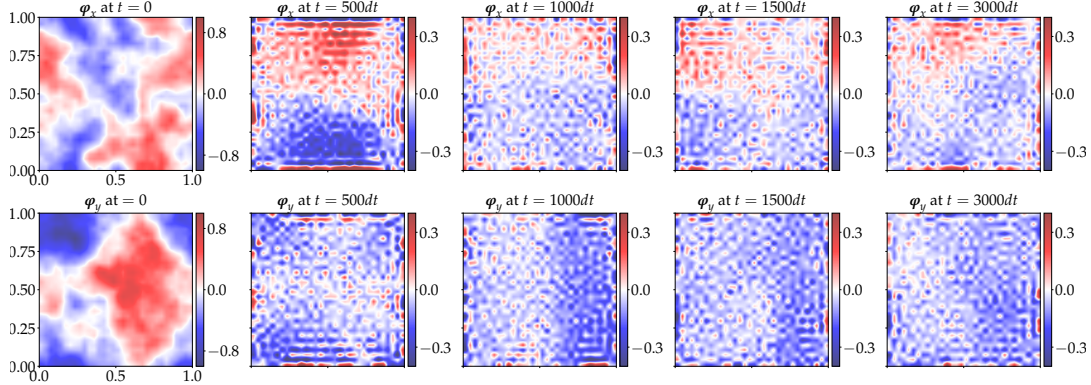
Further, we are interested to find out how much the GPU-compatible design of the Kalman-MPC algorithm improves the computation. To this end, we consider the vector-based version of the algorithm. This variant, referred to as *vector-based Kalman-MPC* in sequel, runs the regular vector-based single-pass EnKS on GPUs after vectorizing (5). Table I offers the comparison of the two versions over different spatial grid sizes. Within the specified GPU-computation setting, the vector-based Kalman-MPC algorithm can achieve control of Burgers' PDE on a grid of up to  $80 \times 80$ , but will run out of

memory beyond this size. By contrast, the GPU-compatible Kalman-MPC algorithm scales well to a  $200 \times 200$  grid. The different memory usage results from the different dimensions of the covariance matrices. If the grid size is  $n \times m$ ,  $\Sigma^{XY}$  is of up to  $nmH \times n$ , and  $\Sigma^Y$  of  $nm \times nm$  for the vector-based Kalman-MPC algorithm; but they are just of  $nH \times n$  and  $n \times n$  for the Kalman-MPC algorithm. Significant difference also arises in the computation time. The GPU-compatible Kalman-MPC algorithm requires much less time, by one order of magnitude, while scalable to the  $200 \times 200$  grid. Our numerous experiments offline have shown that, computation-wise, this algorithm could handle a grid of up to  $500 \times 500$ . But it is hard to train a sufficiently accurate CNN model for this grid, so we skip presenting the results in the paper.

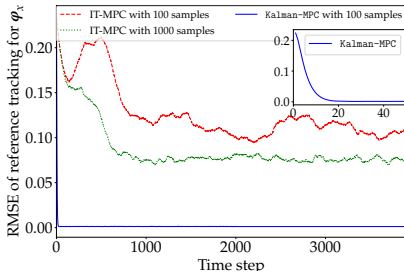
Next, we consider the pointwise control setup to drive  $\varphi$  to zero. Here, the control dimensions are the same as the state dimensions, giving more challenges for computation. For the purpose of comparison, we consider the information-theoretic MPC (IT-MPC) algorithm proposed in [41], which builds upon an information-theoretic interpretation of optimal control, implements sampling-based optimization, and runs on GPUs. After many tries, we find out that the IT-MPC



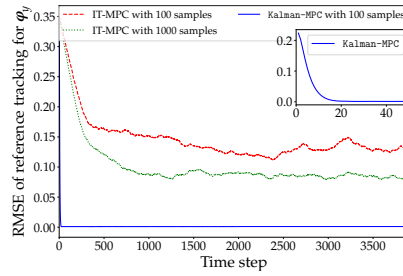
(a) Snapshots of  $\varphi$  on  $200 \times 200$  grid under control by Kalman-MPC with 100 samples.



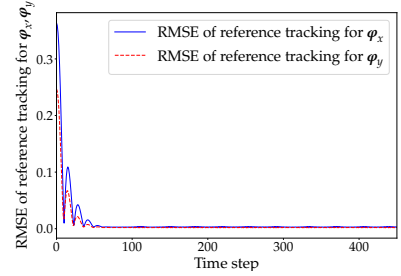
(b) Snapshots of  $\varphi$  on  $32 \times 32$  grid under control by IT-MPC with 1,000 samples.



(c) RMSE for  $\varphi_x$  on  $32 \times 32$  grid by IT-MPC and Kalman-MPC.



(d) RMSE for  $\varphi_y$  on  $32 \times 32$  grid by IT-MPC and Kalman-MPC.



(e) RMSE for  $\varphi_x$  on  $32 \times 32$  grid by Kalman-MPC.

Fig. 3: Comparison between Kalman-MPC and IT-MPC in control of Burgers' PDE.

algorithm can only handle a grid size of at most  $32 \times 32$ . Fig. 3b shows the evolution of the Burger's velocity field in this case, in which the IT-MPC algorithm struggles to accomplish the control objective even though using 1,000 samples. However, the Kalman-MPC algorithm succeeds on a  $200 \times 200$  grid using only 100 samples, as shown in Fig. 3a. Further, the RMSE in reference tracking as shown in Figs. 3c-3e offers a clearer view of the difference, indicating the much better performance by the Kalman-MPC algorithm. The IT-MPC algorithm demonstrates limited scalability, likely because it seeks to search the state and control spaces over the entire horizon. The Kalman-MPC algorithm, in contrast, performs sequential searches at every time step within the horizon, requiring much fewer samples and less computation. Because of the same reason, the Kalman-MPC algorithm requires much less tuning effort to succeed than the IT-MPC does, as consistently shown in our experiments.

## VI. CONCLUSION

Modeling and control of spatio-temporal dynamic systems are critical problems across many domains. CNNs have become increasingly popular for building data-driven models that capture complex spatio-temporal dynamics, but what has been unexplored is optimal control of such CNN-based dynamic models. As a primary challenge, the ultra-high dimensions and nonlinearity intrinsic to CNNs will overwhelm numerical optimization techniques to make the computation prohibitive. In this paper, we propose the optimal inferential control framework to overcome the challenge. We convert the problem of MPC of CNNs into an equivalent probabilistic inference problem. Then, we develop a GPU-compatible EnKS to perform MPC. The resulting algorithm, Kalman-MPC, combines the potency of Monte Carlo sampling with the computing power of GPUs to efficiently infer the best

control decisions despite high-dimensional state and control spaces. Numerical experiments show that the Kalman-MPC algorithm succeeds in controlling spatio-temporal systems with tens of thousands of state and control dimensions. Our study establishes a new way to control spatio-temporal dynamic systems, with potential application to other systems involving high-dimensional nonlinear dynamics.

#### APPENDIX

In this Appendix, we provide a brief overview of random matrices and the matrix normal distribution, which is taken from [45].

A matrix  $X \in \mathbb{R}^{n \times m}$  is a random matrix if its elements are random variables. Its probability density function (pdf)  $p(X)$  satisfies

- 1)  $p(X) \geq 0$ ,
- 2)  $\int_{\Omega} p(X) dX = 1$ , and
- 3)  $P(X \in S) = \int_S p(X) dX$ ,

where  $\Omega$  is the space of realizations of  $X$ , and  $S$  is a subset of  $\Omega$ . If  $X \in \mathbb{R}^{n \times m}$  and  $Y \in \mathbb{R}^{r \times s}$  are two random matrices, their joint pdf  $p(X, Y)$  satisfies

- 1)  $p(X, Y) \geq 0$ ,
- 2)  $\int_{\Omega_{X,Y}} p(X, Y) dX dY = 1$ , and
- 3)  $P((X, Y) \in S) = \int_S p(X, Y) dX dY$ ,

where  $\Omega_{X,Y}$  is the space of realizations of  $(X, Y)$ , and  $S$  is a subset of  $\Omega_{X,Y}$ . The marginal pdf of  $X$  is defined by

$$p(X) = \int_Y p(X, Y) dY,$$

and the conditional pdf is defined by

$$p(X | Y) = \frac{p(X, Y)}{p(Y)}.$$

We say that  $X \in \mathbb{R}^{n \times m}$  has a matrix normal distribution if its pdf is given by

$$p(X) = (2\pi)^{-\frac{nm}{2}} |\Sigma|^{-\frac{n}{2}} |\Psi|^{-\frac{m}{2}} \times \exp \left[ -\frac{1}{2} \text{tr} \left( \Sigma^{-1} (X - M) \Psi^{-1} (X - M)^{\top} \right) \right],$$

where  $M \in \mathbb{R}^{n \times m}$ ,  $\Sigma \in \mathbb{R}^{n \times n} > 0$ , and  $\Psi \in \mathbb{R}^{m \times m} > 0$ . The shorthand notation is

$$X \sim \mathcal{MN}(M; \Sigma, \Psi).$$

It is provable that  $\text{vec}(X^{\top})$  follows a multivariate normal distribution given by

$$\text{vec}(X^{\top}) \sim \mathcal{N}(\text{vec}(M^{\top}); \Sigma \otimes \Psi).$$

The following relations about expected values will hold:

$$\begin{aligned} \mathbb{E}(X) &= M, \\ \mathbb{E} \left[ (X - M)(X - M)^{\top} \right] &= \text{tr}(\Psi)\Sigma, \\ \mathbb{E} \left[ (X - M)^{\top}(X - M) \right] &= \text{tr}(\Sigma)\Psi. \end{aligned}$$

If  $A \in \mathbb{R}^{r \times n}$  and  $B \in \mathbb{R}^{m \times s}$  are of full rank, then

$$AXB \sim \mathcal{MN}(AMB; A\Sigma A^{\top}, B^{\top}\Psi B).$$

If

$$\begin{bmatrix} X_{n \times m} \\ Y_{r \times m} \end{bmatrix} \sim \mathcal{MN} \left( \begin{bmatrix} M_X \\ M_Y \end{bmatrix}; \begin{bmatrix} \Sigma_X & \Sigma_{XY} \\ \Sigma_{XY}^{\top} & \Sigma_Y \end{bmatrix}, \Psi \right),$$

then

$$X | Y \sim \mathcal{MN} \left( M_X + \Sigma_{XY} \Sigma_Y^{-1} (Y - M_Y); \Sigma_X - \Sigma_{XY} \Sigma_Y^{-1} \Sigma_{XY}^{\top}, \Psi \right).$$

#### REFERENCES

- [1] Han-Xiong Li and Chenkun Qi. *Spatio-Temporal Modeling of Nonlinear Distributed Parameter Systems*. Springer Dordrecht, 2011.
- [2] Salvatore Cuomo, Vincenzo Schiano Di Cola, Fabio Giampaolo, Gianluigi Rozza, Maziar Raissi, and Francesco Piccialli. Scientific machine learning through physics-informed neural networks: Where we are and what's next. *Journal of Scientific Computing*, 92(3):88, 2022.
- [3] Christopher K Wikle and Andrew Zammit-Mangion. Statistical deep learning for spatial and spatiotemporal data. *Annual Review of Statistics and Its Application*, 10:247–270, 2023.
- [4] George Em Karniadakis, Ioannis G. Kevrekidis, Lu Lu, Paris Perdikaris, Sifan Wang, and Liu Yang. Physics-informed machine learning. *Nature Review Physics*, 3(88):422–440, 2021.
- [5] Ashesh Chattopadhyay, Pedram Hassanzadeh, and Saba Pasha. Predicting clustered weather patterns: A test case for applications of convolutional neural networks to spatio-temporal climate data. *Scientific Reports*, 2020.
- [6] Junbo Zhang, Yu Zheng, and Dekang Qi. Deep spatio-temporal residual networks for citywide crowd flows prediction. In *Proceedings of the 31st AAAI Conference on Artificial Intelligence*, page 1655–1661, 2017.
- [7] Saakaar Bhatnagar, Yaser Afshar, Shaowu Pan, Karthik Duraisamy, and Shailendra Kaushik. Prediction of aerodynamic flow fields using convolutional neural networks. In *Computational Mechanics*, volume 64, page 525–545, 2019.
- [8] A. Smyshlyaev and M. Krstic. Closed-form boundary state feedbacks for a class of 1-D partial integro-differential equations. *IEEE Transactions on Automatic Control*, 49(12):2185–2202, 2004.
- [9] Miroslav Krstic and Andrey Smyshlyaev. *Boundary Control of PDEs*. SIAM, 2008.
- [10] Jean-Michel Coron, Rafael Vazquez, Miroslav Krstic, and Georges Bastin. Local exponential  $H^2$  stabilization of a  $2 \times 2$  quasilinear hyperbolic system using backstepping. *SIAM Journal on Control and Optimization*, 51(3):2005–2035, 2013.
- [11] B.-Z. Guo and J.-M. Wang. *Control of Wave and Beam PDEs*. Springer Cham, 2019.
- [12] J.-M. Coron, B. d'Andrea Novel, and G. Bastin. A strict Lyapunov function for boundary control of hyperbolic systems of conservation laws. *IEEE Transactions on Automatic Control*, 2007.
- [13] J. L. Lions. The optimal control of distributed systems. *Russian Mathematical Surveys*, 28(4):13–46, 1973.
- [14] Alain Bensoussan, Giuseppe Da Prato, Michel C. Delfour, and Sanjoy K. Mitter. *Representation and Control of Infinite Dimensional Systems*. Birkhäuser Boston, 2007.
- [15] Ilyasse Aksikas, Adrian Fuxman, J. Fraser Forbes, and Joseph J. Winkin. LQ control design of a class of hyperbolic PDE systems: Application to fixed-bed reactor. *Automatica*, 45(6):1542–1548, 2009.
- [16] Chao Xu, Yongsheng Ou, and Eugenio Schuster. Sequential linear quadratic control of bilinear parabolic PDEs based on POD model reduction. *Automatica*, 47(2):418–426, 2011.
- [17] Aditya Gahlawat and Matthew M. Peet. A convex sum-of-squares approach to analysis, state feedback and output feedback control of parabolic PDEs. *IEEE Transactions on Automatic Control*, 62(4):1636–1651, 2017.
- [18] P. Dufour, D.J. Michaud, Y. Touré, and P.S. Dhurjati. A partial differential equation model predictive control strategy: Application to autoclave composite processing. *Computers & Chemical Engineering*, 28(4):545–556, 2004.
- [19] Lars Grüne, Manuel Schaller, and Anton Schiela. Sensitivity analysis of optimal control for a class of parabolic PDEs motivated by model predictive control. *SIAM Journal on Control and Optimization*, 57(4):2753–2774, 2019.



- [20] Hassan Arbabi, Milan Korda, and Igor Mezić. A data-driven Koopman model predictive control framework for nonlinear partial differential equations. In *2018 IEEE Conference on Decision and Control (CDC)*, pages 6409–6414. IEEE, 2018.
- [21] Milan Korda and Igor Mezić. Linear predictors for nonlinear dynamical systems: Koopman operator meets model predictive control. *Automatica*, 93:149–160, 2018.
- [22] Jeremy Morton, Antony Jameson, Mykel J Kochenderfer, and Freddie Witherden. Deep dynamical modeling and control of unsteady fluid flows. *Advances in Neural Information Processing Systems*, 31, 2018.
- [23] Svein Hovland, Jan Tommy Gravdahl, and Karen E. Willcox. Explicit model predictive control for large-scale systems via model reduction. *Journal of Guidance, Control, and Dynamics*, 31(4):918–926, 2008.
- [24] Sebastian Peitz and Stefan Klus. Koopman operator-based model reduction for switched-system control of PDEs. *Automatica*, 106:184–191, 2019.
- [25] A. Draeger, S. Engell, and H. Ranke. Model predictive control using neural networks. *IEEE Control Systems Magazine*, 15(5):61–66, 1995.
- [26] S. Piche, B. Sayyar-Rodsari, D. Johnson, and M. Gerules. Nonlinear model predictive control using neural networks. *IEEE Control Systems Magazine*, 20(3):53–62, 2000.
- [27] Maciej Ławryńczuk. *MPC Algorithms Based on Neural State-Space Models*, page 139–166. Springer International Publishing, 2014.
- [28] Alberto Bemporad. A piecewise linear regression and classification algorithm with application to learning and model predictive control of hybrid systems. *IEEE Transactions on Automatic Control*, 68(6):3194–3209, 2023.
- [29] J. Pohlodek, H. Alsmeier, B. Morabito, C. Schlauch, A. Savchenko, and R. Findeisen. Stochastic model predictive control utilizing Bayesian neural networks. In *Proceedings of American Control Conference*, pages 603–608, 2023.
- [30] Francesco Cursi, Valerio Modugno, Leonardo Lanari, Giuseppe Oriolo, and Petar Kormushev. Bayesian neural network modeling and hierarchical MPC for a tendon-driven surgical robot with uncertainty minimization. *IEEE Robotics and Automation Letters*, 6(2):2642–2649, 2021.
- [31] Tim Salzmann, Elia Kaufmann, Jon Arrizabalaga, Marco Pavone, Davide Scaramuzza, and Markus Ryll. Real-time neural MPC: Deep learning model predictive control for quadrotors and agile robotic platforms. *IEEE Robotics and Automation Letters*, 8(4):2397–2404, 2023.
- [32] Felix Bunning, Adrian Schalbetter, Ahmed Aboudonia, Mathias Hudoba de Badyn, Philipp Heer, and John Lygeros. Input convex neural networks for building MPC. In *Proceedings of the 3rd Conference on Learning for Dynamics and Control*, volume 144, pages 251–262, 2021.
- [33] Anusha Nagabandi, Gregory Kahn, Ronald S. Fearing, and Sergey Levine. Neural network dynamics for model-based deep reinforcement learning with model-free fine-tuning. In *Proceedings of IEEE International Conference on Robotics and Automation*, page 7559–7566, 2018.
- [34] Iman Askari, Shen Zeng, and Huazhen Fang. Nonlinear model predictive control based on constraint-aware particle filtering/smoothing. In *Proceedings of the American Control Conference*, pages 3532–3537, 2021.
- [35] Iman Askari, Babak Badnava, Thomas Woodruff, Shen Zeng, and Huazhen Fang. Sampling-based nonlinear MPC of neural network dynamics with application to autonomous vehicle motion planning. In *Proceedings of the American Control Conference*, pages 2084–2090, 2022.
- [36] Iman Askari, Xumein Tu, Shen Zeng, and Huazhen Fang. Model predictive inferential control of neural state-space models for autonomous vehicle motion planning, 2023.
- [37] R. E. Kalman. A new approach to linear filtering and prediction problems. *Journal of Basic Engineering*, 82(1):35–45, 1960.
- [38] Emanuel Todorov. General duality between optimal control and estimation. In *2008 47th IEEE Conference on Decision and Control*, pages 4286–4292, 2008.
- [39] Emanuel Todorov. Efficient computation of optimal actions. *Proceedings of the National Academy of Sciences*, 106(28):11478–11483, 2009.
- [40] Jin W. Kim and Prashant G. Mehta. Duality for nonlinear filtering II: optimal control. *IEEE Transactions on Automatic Control*, 2023. in press.
- [41] Grady Williams, Paul Drews, Brian Goldfain, James M Reh, and Evangelos A Theodorou. Information-theoretic model predictive control: Theory and applications to autonomous driving. *IEEE Transactions on Robotics*, 34(6):1603–1622, 2018.
- [42] Hilbert J. Kappen, Vicenc Gomez, and Manfred Opper. Optimal control as a graphical model inference problem. *Machine Learning*, 2012.
- [43] Dominik Stahl and Jan Hauth. PF-MPC: Particle filter-model predictive control. *Systems & Control Letters*, 60(8):632–643, 2011.
- [44] Sergey Levine. Reinforcement Learning and Control as Probabilistic Inference: Tutorial and Review, 2018. arXiv:1805.00909 [cs, stat].
- [45] Arjun K Gupta and Daya K Nagar. *Matrix Variate Distributions*. Chapman and Hall/CRC, 2018.
- [46] Matthias Katzfuss, Jonathan R Stroud, and Christopher K Wikle. Ensemble Kalman methods for high-dimensional hierarchical dynamic space-time models. *Journal of the American Statistical Association*, 2019.
- [47] Geir Evensen and Peter Jan Van Leeuwen. An ensemble Kalman smoother for nonlinear dynamics. *Monthly Weather Review*, 128(6):1852–1867, 2000.
- [48] Pu Ren, Chengping Rao, Yang Liu, Jian-Xun Wang, and Hao Sun. PhyCRNet: Physics-informed convolutional-recurrent network for solving spatiotemporal pdes. *Computer Methods in Applied Mechanics and Engineering*, 389, 2022.